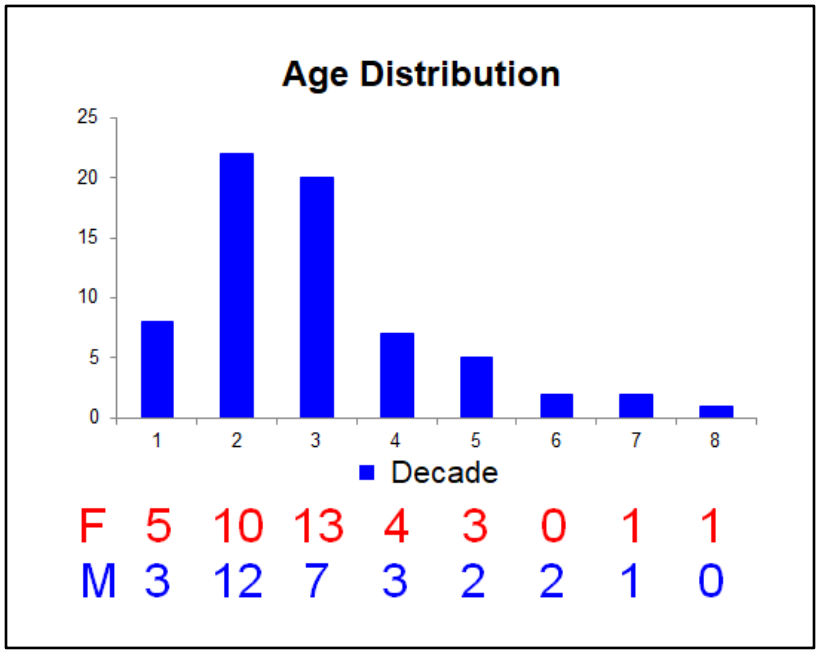

Figure S1: Age and gender distribution of PXA patients
Age at first diagnosis is shown for 67 patients. M, Male; F, Female

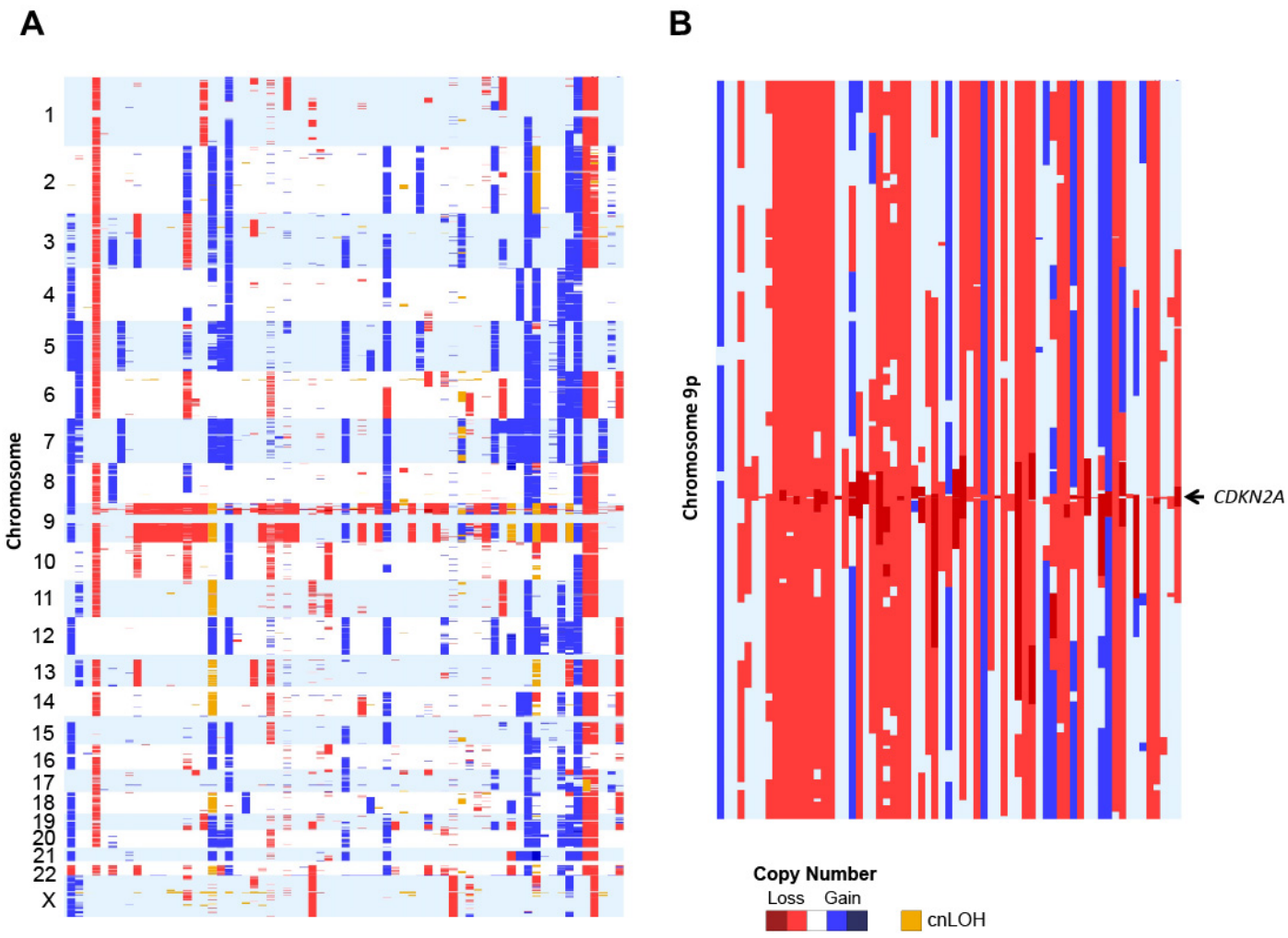

Figure S2: Copy number alterations in PXA

(A) Genome-wide copy number alterations. (B) Copy number alterations of 9p, highlighting homozygous deletions of *CDKN2A/B.* Case order matches that of Figure 1. cnLOH, copy neutral loss of heterozygosity

Case 14

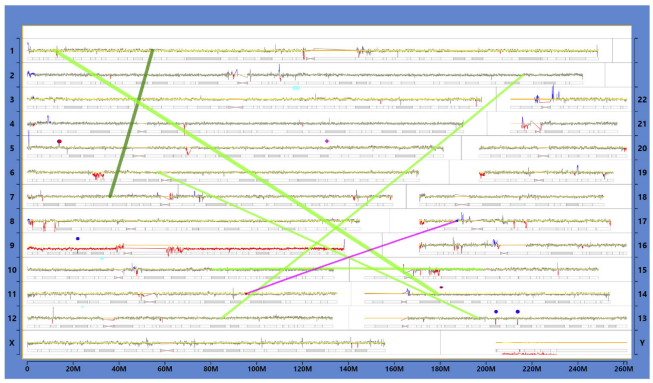

Case 45

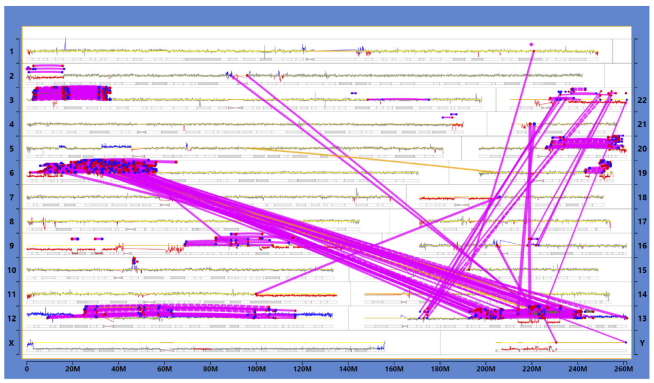

Case 51

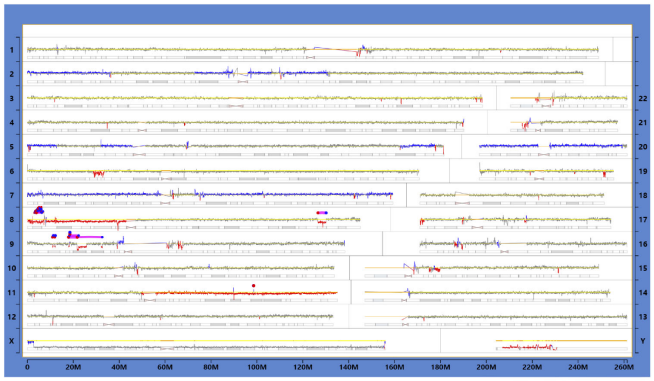

Case 55

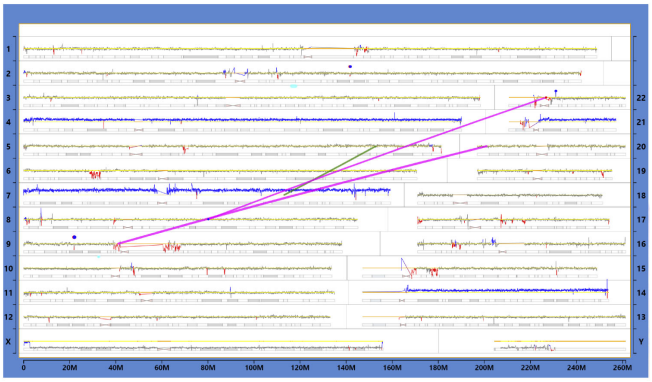

Case 58

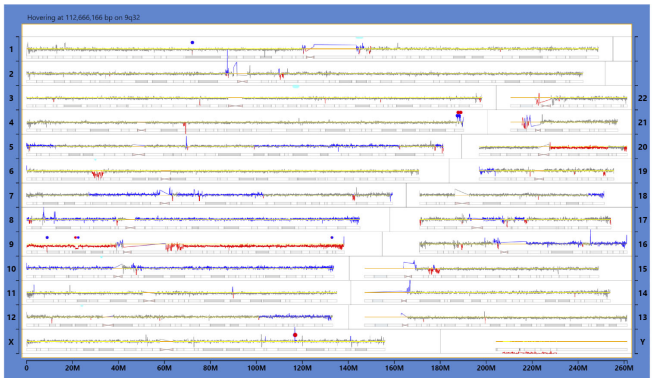

Case 64

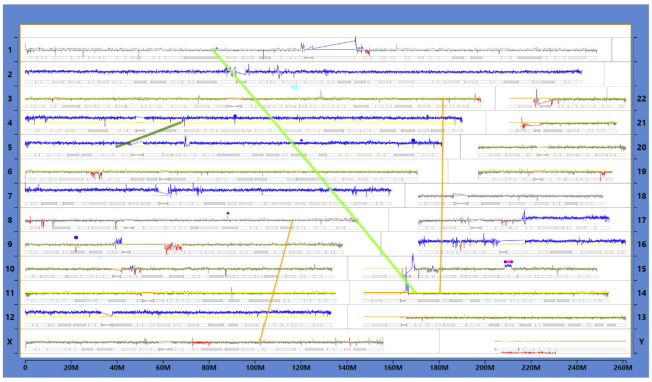

Figure S3: Structural rearrangements determined by mate-pair sequencing
Genome U-plots are shown with chromosomes plotted in order of size as denoted on the y-axes. Copy number gains are shown in blue and losses in red. Structural rearrangements are depicted as connecting lines, with unbalanced translocations in magenta, balanced translations in dark green, transposons in light green, and complex or ambiguous rearrangements in orange. For unbalanced translocations, red or blue ends denote reads mapped to reverse or forward strand, respectively.

A

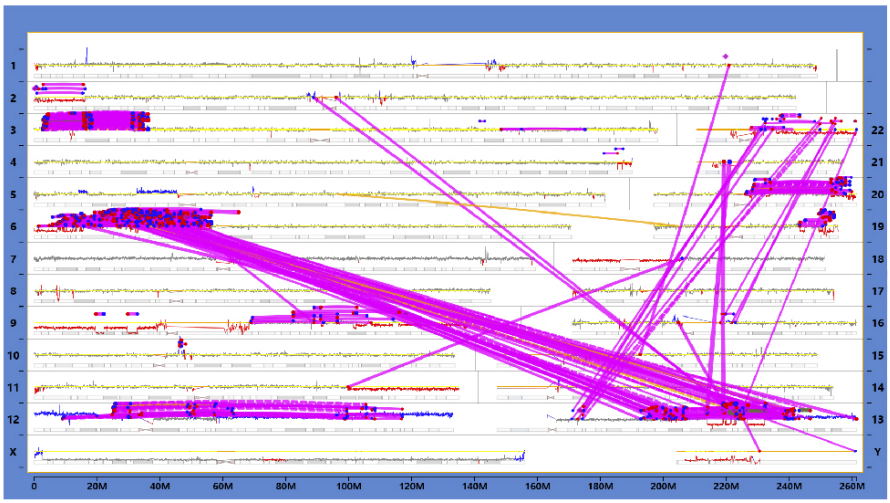

B

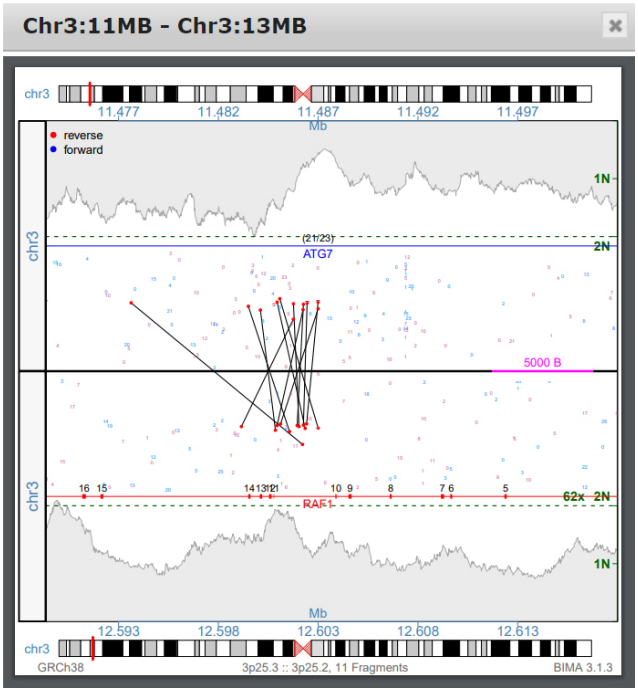

Figure S4: Structural rearrangements of case 45

(A) Genome plot of case 45. Complex structural rearrangements were identified, including chromoplexis involving chromosomes 6, 13, 16, and 22. (B) Junction plot demonstrating *ATG7-RAF1* fusion. The fusion involved intronic regions resulting in fusion of *ATG7* exons 1-18 with *RAF1* exons 11-17.

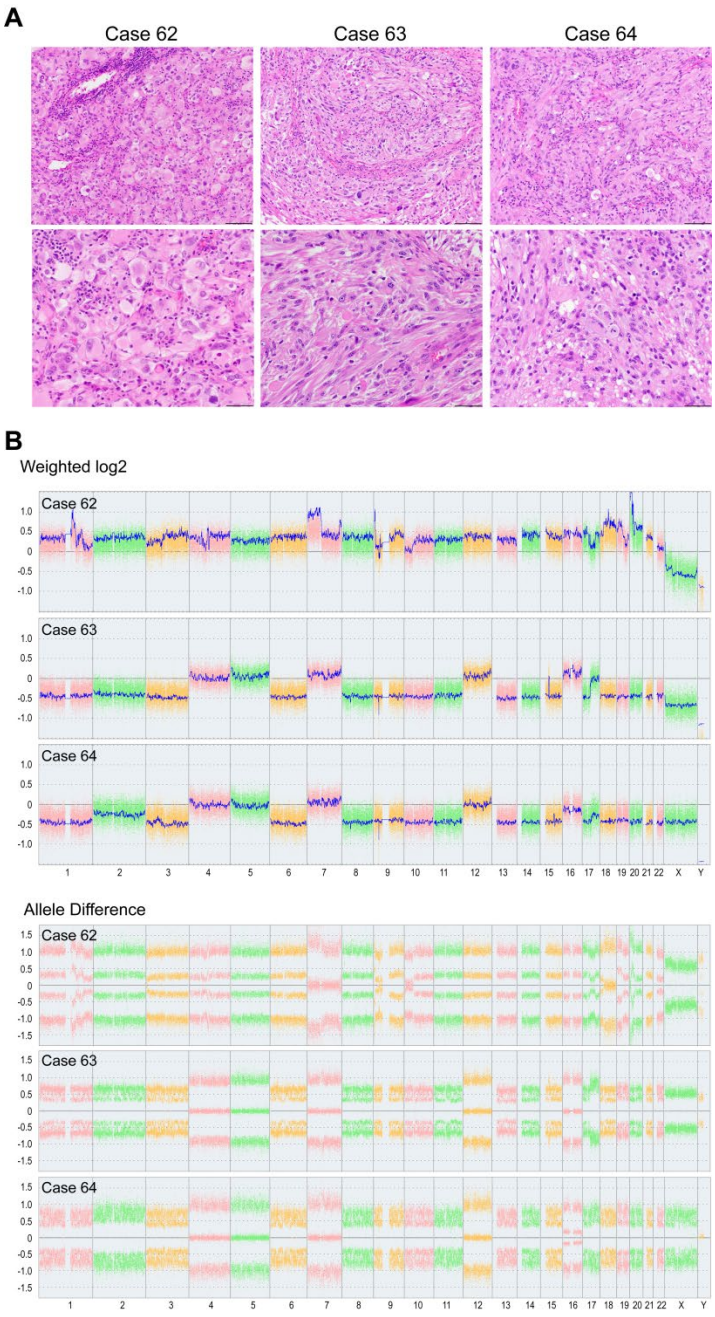

Figure S5: Histology and copy number profiles of *NF1*-mutant A-PXA
(A) Morphology of *NF1*-mutant A-PXA. Case 62 showed a predominance of large, pleomorphic and variably lipidized cells, with prominent perivascular inflammation. Cases 63 and 64 showed prominent spindled morphology, admixed with pleomorphic and scattered xanthomatous cells. All cases demonstrated >5 mitoses per 10 high-power fields. Case 63 also showed necrosis and case 42 both necrosis and microvascular proliferation. H&E photomicrographs shown at 200x (top panel; scale bar = 100 μM) and 400x (bottom, scale bar = 50 μM) magnification. (B) Genome-wide copy number profiles of *NF1*-mutant A-PXA. Case 62 showed an apparently triploid genome with many additional complex CNVs. Cases 63 and 64 showed a nearly identical pattern of CNVs, with a near haploid genotype and homozygous deletion of *CDKN2A/B*.

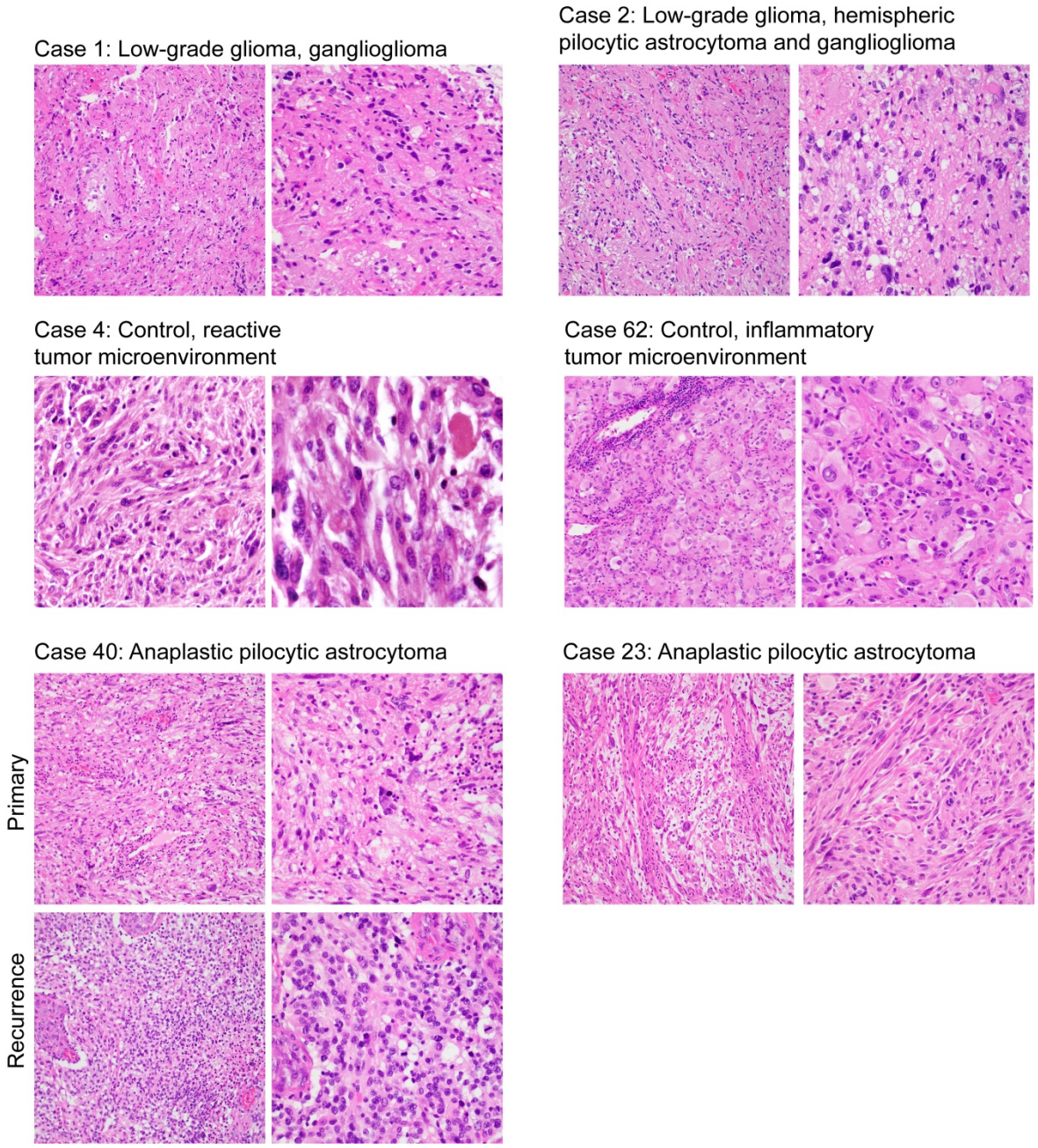

Figure S6: Histology of PXA clustering with other reference groups

Cases 1 and 2 demonstrated pleomorphic, low-grade gliomas. No apparent ganglion cell component was identified by immunohistochemistry (not shown). Case 2 showed numerous eosinophilic granular bodies and was more cellular than typical of pilocytic astrocytoma. Cases 4 and 62 showed cellular tumor consistent with PXA. Cases 41 and 23 were cerebellar tumors with spindled and pleomorphic components. Case 40 is shown at initial resection and at recurrence. The recurrent tumor was high-grade and unrecognizable as a PXA, with small cell morphology, necrosis, and microvascular proliferation. H&E photomicrographs shown at 200x (left panel) and 400x (right panel) for each case.

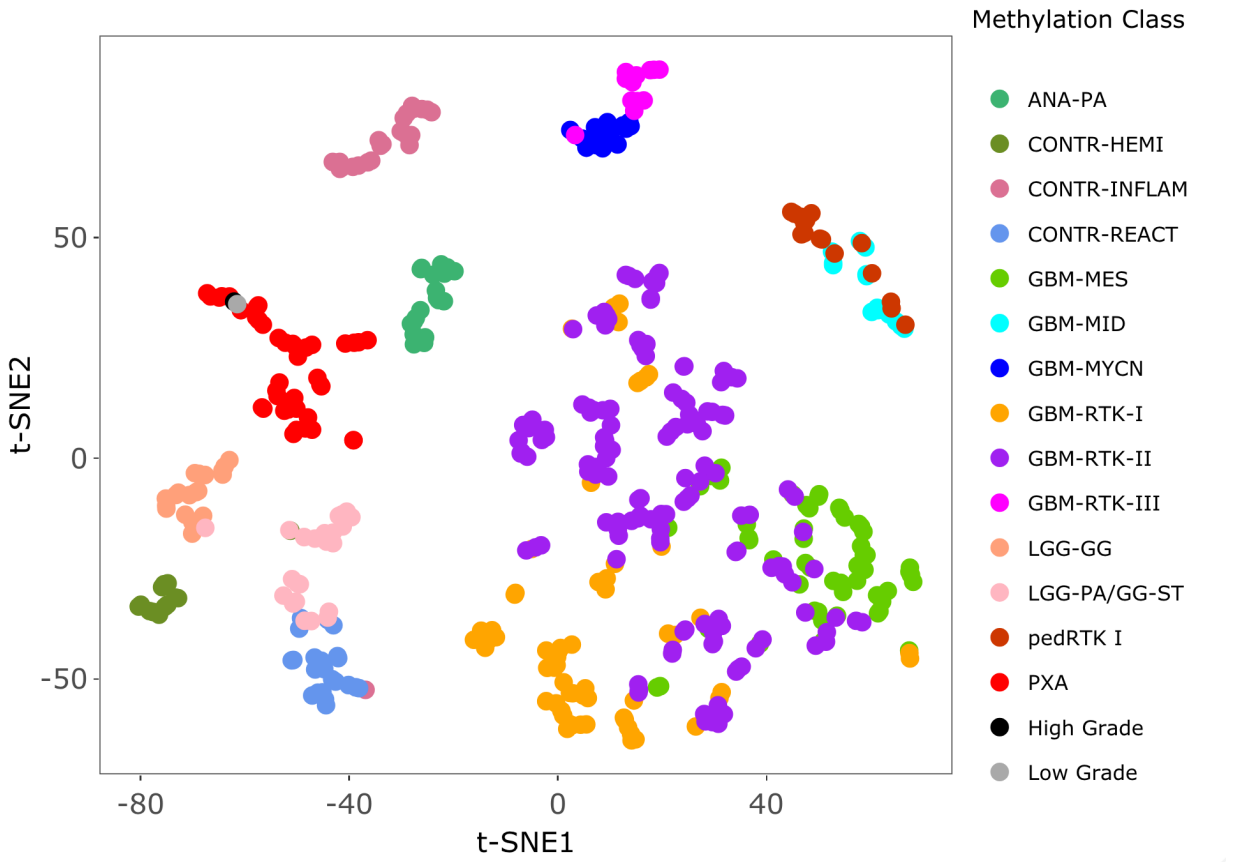

Figure S7: t-SNE of distinct low- and high-grade areas of case 67

Histologically low-grade (grey) and high-grade (black) components from case 67 were analyzed independently by methylation profiling. Reference methylation classes included: PXA, (anaplastic) pleomorphic xanthoastrocytoma; ANA PA, anaplastic pilocytic astrocytoma; LGG-GG, low-grade glioma, ganglioglioma; LGG-PA/GG-ST, low-grade glioma, subclass hemispheric pilocytic astrocytoma and ganglioglioma; CONT-INFLAM, control tissue, inflammatory tumor microenvironment; CONT-HEMI, control tissue hemispheric cortex; CONT-REACT, control tissue, reactive tumor microenvironment; glioblastoma IDH wildtype subgroups: GBM-MES, mesenchymal subclass; GBM-MID, midline subclass; GBM-RTK-I subclass; GBM RTK-II subclass; GBM-RTK-III subclass; pedRTK I subclass; GBM-MYCN subclass.